

## Supporting Information

### **Zeolite-Templated Carbon as the Cathode for a High Energy Density Dual-Ion Battery**

Romain J.-C. Dubey<sup>†‡</sup>, Jasmin Nüssli<sup>†‡</sup>, Laura Piveteau<sup>†‡</sup>, Kostiantyn V. Kravchyk<sup>†‡</sup>, Marta D. Rossell<sup>||</sup>, Marco Campanini<sup>||</sup>, Rolf Erni<sup>||</sup>, Maksym V. Kovalenko<sup>†‡\*</sup>, and Nicholas P. Stadie<sup>#\*</sup>

<sup>†</sup>Laboratory of Inorganic Chemistry, Department of Chemistry and Applied Biosciences, ETH Zürich, CH-8093 Zürich, Switzerland

<sup>‡</sup>Laboratory for Thin Films and Photovoltaics, Empa, Swiss Federal Laboratories for Materials Science & Technology, CH-8600 Dübendorf, Switzerland

<sup>||</sup>Electron Microscopy Center, Empa, Swiss Federal Laboratories for Materials Science & Technology, CH-8600 Dübendorf, Switzerland

<sup>#</sup>Department of Chemistry & Biochemistry, Montana State University, Bozeman, Montana, 59717, United States

\* nstadie@montana.edu, mvkovalenko@ethz.ch

## Contents:

- Figure S1. SEM imaging of ZTC and zeolite NaY  
Figure S2. TEM imaging of ZTC  
Figure S3. Structural comparison between TEM images and molecular model of ZTC  
Figure S4. BET plot of nitrogen adsorption on ZTC (and other materials)  
Figure S5. DR plot of nitrogen adsorption on ZTC (and other materials)  
Figure S6. Surface area and micropore analysis of cathode materials for KFSI DIBs
- Figure S7. Capacity and efficiency of ZTC in KFSI electrolyte of varying concentration  
Figure S8. Cyclic voltammetry of ZTC in KFSI electrolyte within different voltage ranges  
Figure S9. Single discharge experiment of ZTC in KFSI electrolyte  
Figure S10. Cyclic voltammetry of ZTC in KFSI electrolyte within the optimized range
- Figure S11. Galvanostatic cycling of ZTC during pretreatment in KFSI electrolyte  
Figure S12. Galvanostatic cycling of ZTC as an anode in KFSI electrolyte
- Figure S13.  $^{19}\text{F}$  static NMR comparison between pristine and cycled ZTC  
Figure S14.  $^{13}\text{C}$  MAS NMR comparison between pristine and cycled ZTC  
Tables S1-S4. Acquisition parameters for all  $^{19}\text{F}$  and  $^{13}\text{C}$  NMR experiments
- Table S5. Elemental analysis of impregnated and cycled ZTC  
Figure S15. Elemental analysis diagram of impregnated and cycled ZTC
- Figure S16. Cathodic energy/power densities of ZTC as a function of current rate  
Figure S17. Schematic description of the working principle of a ZTC KFSI DIB  
Table S6. Full-cell gravimetric energy/power density calculations for ZTC KFSI DIBs  
Figure S18. Schematic diagram of relative quantities of electrolyte and ZTC in KFSI DIBs  
Table S7. Bulk material densities for gravimetric to volumetric density calculations  
Tables S8-S9. Full-cell volumetric energy/power density calculations for ZTC KFSI DIBs

## **Zeolite-Templated Carbon (ZTC)**

The optimized synthesis route to zeolite-templated carbon (ZTC) has recently been reviewed elsewhere<sup>S1</sup>; in this work, the well-established two-step<sup>S2,S3</sup> (liquid phase followed by vapor phase) impregnation method is employed, and structural fidelity is further improved by the use of a low-pressure CVD technique. The high template fidelity FAU-ZTC product is confirmed primarily by powder X-ray diffraction (showing an intense (111) reflection at d-spacing = 1.36 nm) and N<sub>2</sub> adsorption (exhibiting a BET surface area of >3300 m<sup>2</sup> g<sup>-1</sup>), as well as by SEM and TEM imaging.

### **Synthesis of ZTC**

The zeolite NaY template (HSZ 320NAA, Tosoh Corp.) was degassed at 300 °C for 24 h under rough vacuum ( $<2 \times 10^{-3}$  mbar) and stored under dry argon atmosphere. Then, 2 g of dried zeolite were combined with 10 mL of furfuryl alcohol (FA, 99%, Aldrich) in a dry argon glovebox ( $<0.5$  ppm O<sub>2</sub>/H<sub>2</sub>O) and the mixture was stirred at room temperature for 24 h. The impregnated solid was then collected by vacuum filtration in air, washed three times with 10 mL aliquots of mesitylene (97%, Aldrich), and dried under suction on the filter frit for 15 min. The impregnated and rinsed zeolite was then placed in an alumina boat (10×30×107 mm) which was inserted into a custom quartz tube (ø 35 mm, open on one end) and installed in a horizontal tube furnace (FST 13/70/500, Carbolite Gero) with a custom vacuum fitting allowing gas flow into and out of the tube over the sample. The tube was evacuated and refilled with dry argon up to 1 mbar and held under flow at 200 sccm. The FA within the zeolite pores was first polymerized by heating up to 150 °C via a 2 h ramp and held for 12 h. The poly-FA was then carbonized by heating up to 700 °C via a 2 h ramp and held for 1 h. Further impregnation was accomplished via propylene CVD at 700 °C; the gas flow was switched to 7 mol% propylene in nitrogen (99.999%, Messer Schweiz AG) at 200 sccm and the outflow was throttled to achieve a constant pressure of 205±5 mbar in the deposition zone. After low-pressure CVD for 3 h, the gas flow was returned to dry argon at 200 sccm and 1 mbar pressure. An annealing step was performed by heating the zeolite-carbon composite up to 900 °C via a 1 h ramp, and held for an additional 3 h. The system was then cooled overnight, the gas flow was stopped, and the annealed zeolite-carbon composite was removed. Removal of the zeolite template was accomplished by three sequential dissolutions in 45 mL of aqueous hydrofluoric acid (HF, 40%, Sigma-Aldrich), followed each time by rinsing in distilled water. The final ZTC product was collected by centrifugation, washed five times with 50 mL aliquots of distilled water, and then dried in air at 80 °C. Prior to electrode preparation and characterization, the ZTC was further dried/degassed at 200 °C under rough vacuum (10<sup>-3</sup> mbar) for 12 h to obtain “pristine ZTC.”

## SEM Imaging of ZTC

Scanning electron microscopy (SEM) of pristine ZTC shows regularly shaped particles identical in morphology and size to the zeolite NaY template (**Figure S1**).

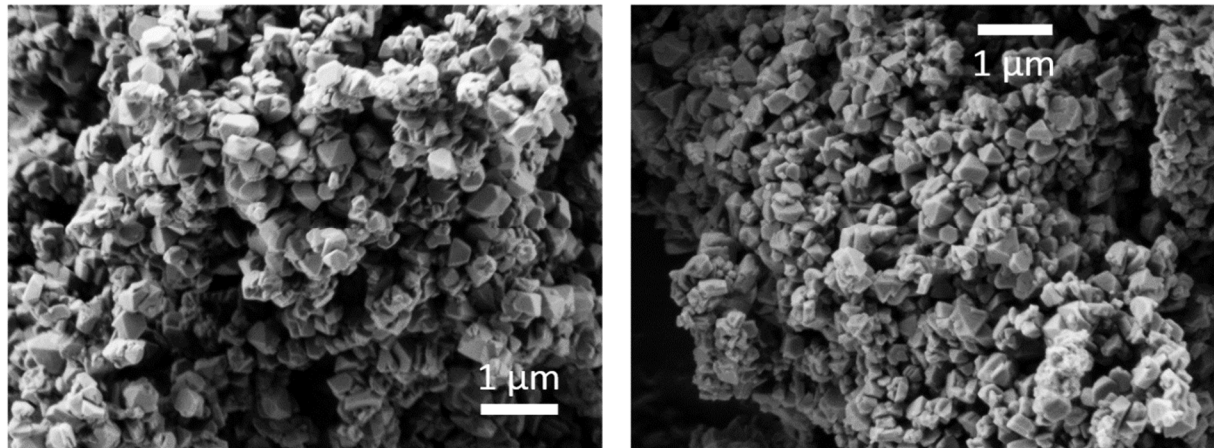


**Figure S1.** Scanning electron micrographs of microcrystalline zeolite NaY (left) and pristine ZTC after template removal (right).

## TEM Analysis of ZTC

Transmission electron microscopy (TEM) of pristine ZTC (when in a thin enough region and in the correct orientation with respect to the electron beam) shows the ordering of the 111 planes as detected by X-ray diffraction, with a characteristic repeat distance of 1.4 nm over large distances of up to 0.1-0.5 μm (**Figure S2**). This ordering is consistent with the recently updated molecular structure<sup>S4</sup> of faujasite-type ZTC (referred to as “Model II” by Nishihara et al.), as shown by overlay of the molecular model (yellow) onto the TEM data (grayscale) at the same length scale (**Figure S3**).

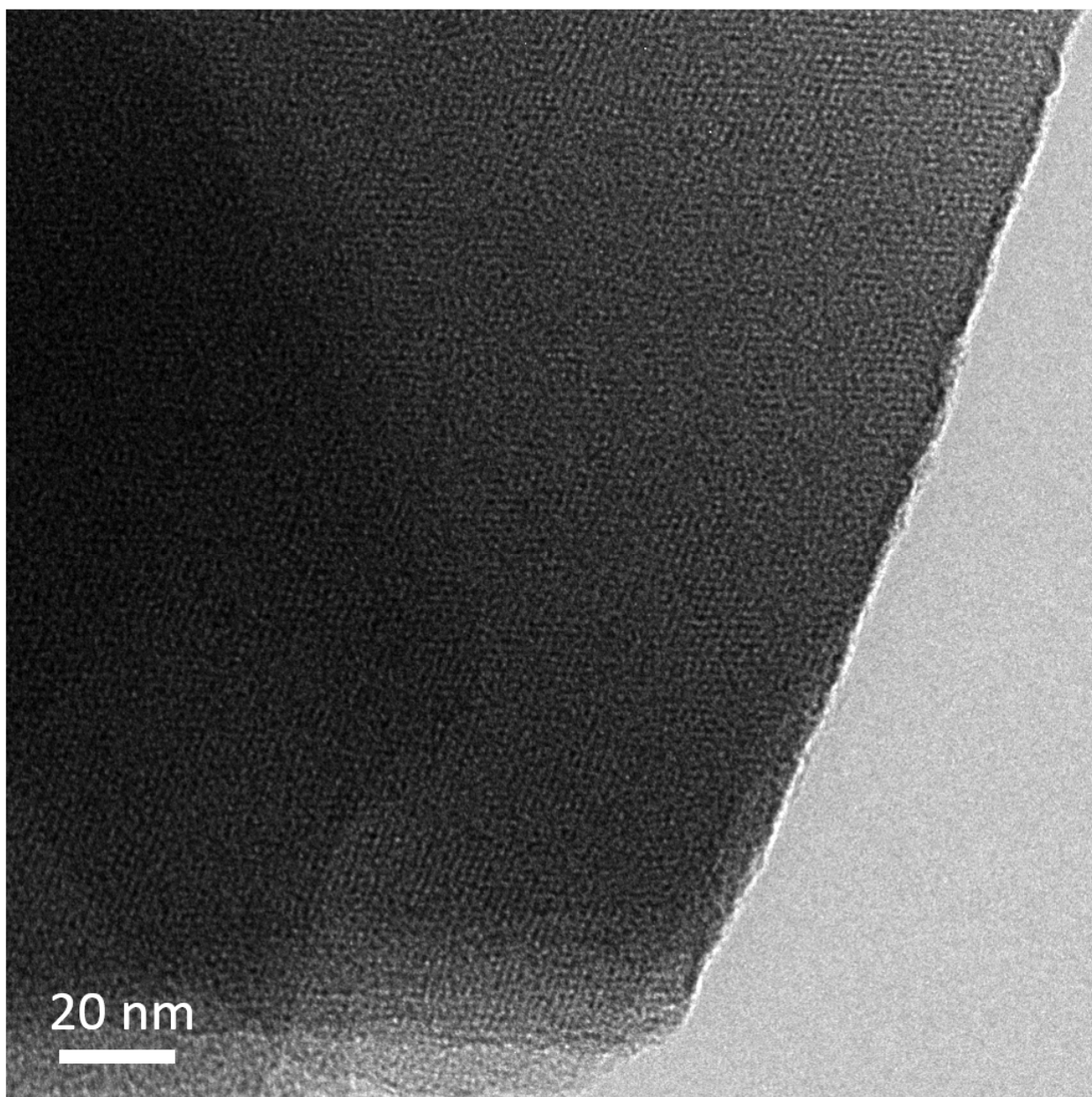


**Figure S2.** Zero-loss filtered transmission electron micrograph of pristine ZTC showing high pore-to-pore regularity across the entire particle.

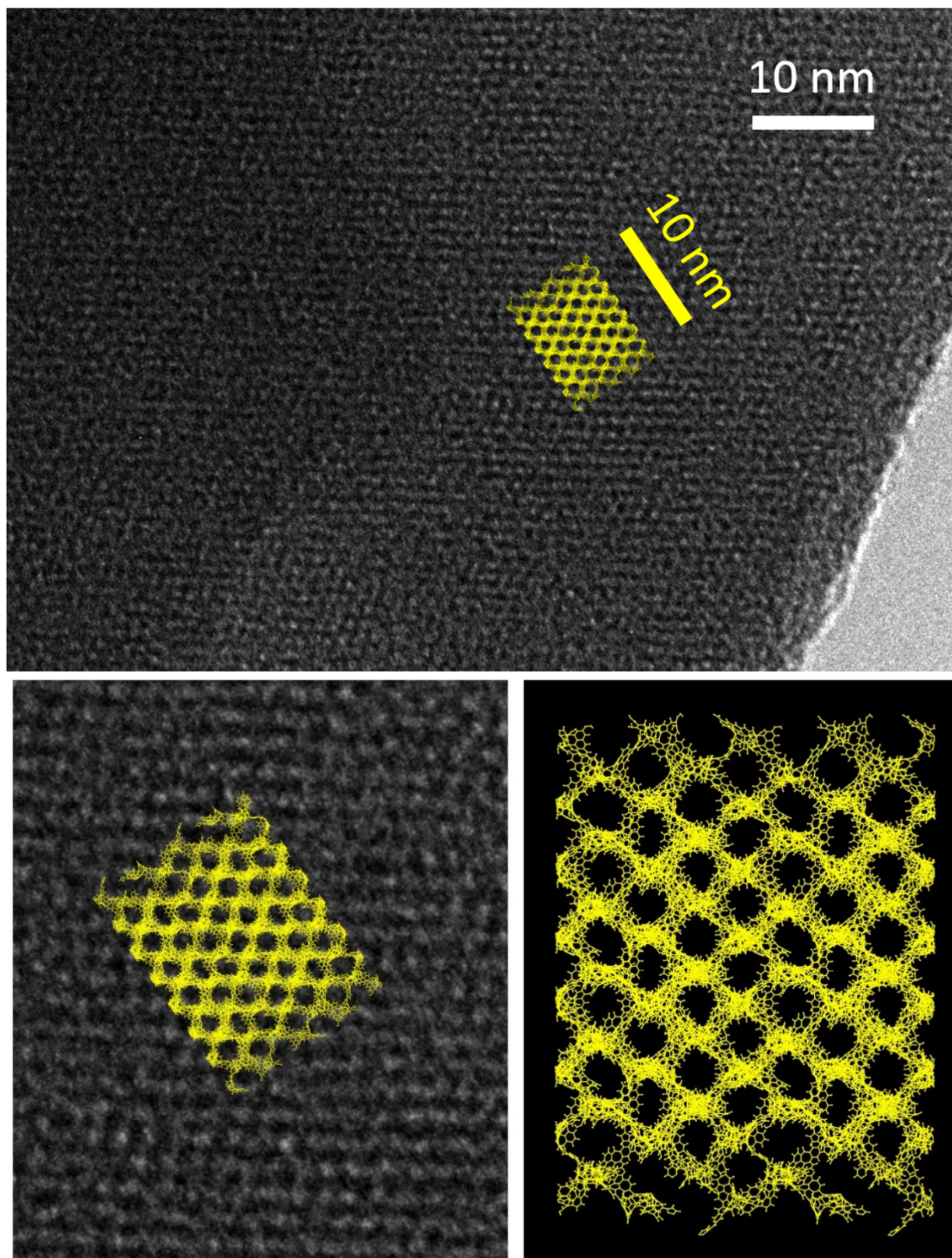


**Figure S3.** Zero-loss filtered transmission electron micrograph of pristine ZTC (grayscale) overlaid by a rescaled molecular model of FAU-ZTC (yellow, referred to as “Model II”<sup>S4</sup>).

## Other Porous Carbon Materials

Several other ordered porous carbon materials were obtained for comparison to ZTC. Two mesoporous templated carbons (MTC21 and MTC31) were prepared and have been previously described.<sup>S5</sup> A commercial ordered mesoporous carbon CMK-3 (ACS Material, LLC) was also investigated, and characterized below.

## Porosity and Surface Area Measurements

Equilibrium nitrogen adsorption and desorption isotherms at 77 K were measured on all porous carbon samples investigated for use as the active cathode material in KFSI DIBs. Standard analysis methods<sup>S6</sup> were used to estimate the specific surface area and total micropore volume of each material for comparison to their corresponding electrochemical performance in functioning DIB cells. The Brunauer-Emmett-Teller (BET) method is a conventional method used to characterize the surface area of porous materials despite its well-known shortcomings for materials containing predominantly micropores (by following the relevant consistency criteria<sup>S7</sup>). Likewise, the Dubinin-Radushkevich (DR) model was employed to determine the micropore volume of each material per conventional methods.

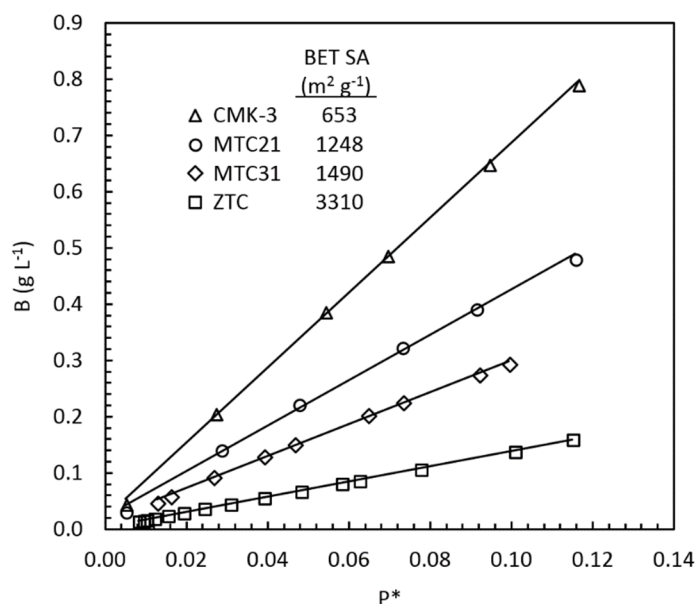


**Figure S4.** Brunauer-Emmett-Teller (BET) plot of N<sub>2</sub> adsorption uptake on ZTC at 77 K for comparison to MTC21, MTC31, and commercially obtained CMK-3, where  $P^* = P/P_0$  and the BET linearized variable is  $B = P^*/(1-P^*)/(v_{STP})$ . The calculated BET surface areas are also shown.

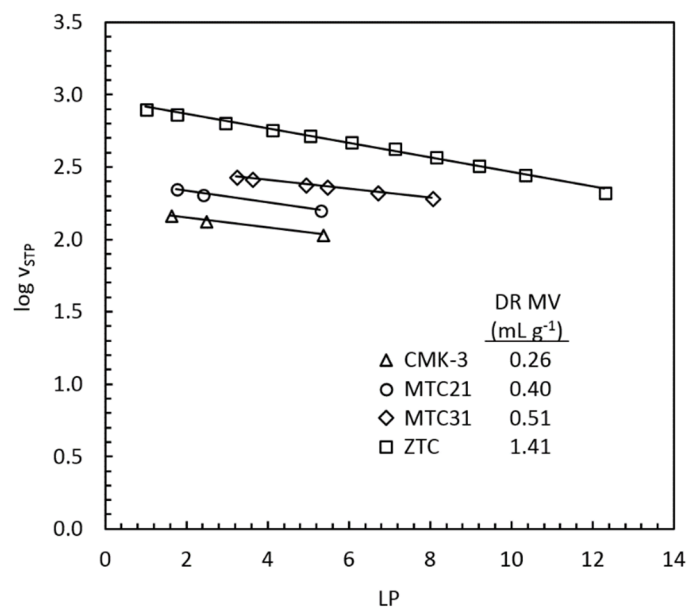


**Figure S5.** Dubinin-Radushkevich (DR) plot of N<sub>2</sub> adsorption on ZTC at 77 K, for comparison to MTC21, MTC31, and commercially obtained CMK-3, where  $LP = (\log (1/P^*))^2$  and  $P^* = P/P_0$ . The calculated DR micropore volumes are also shown.

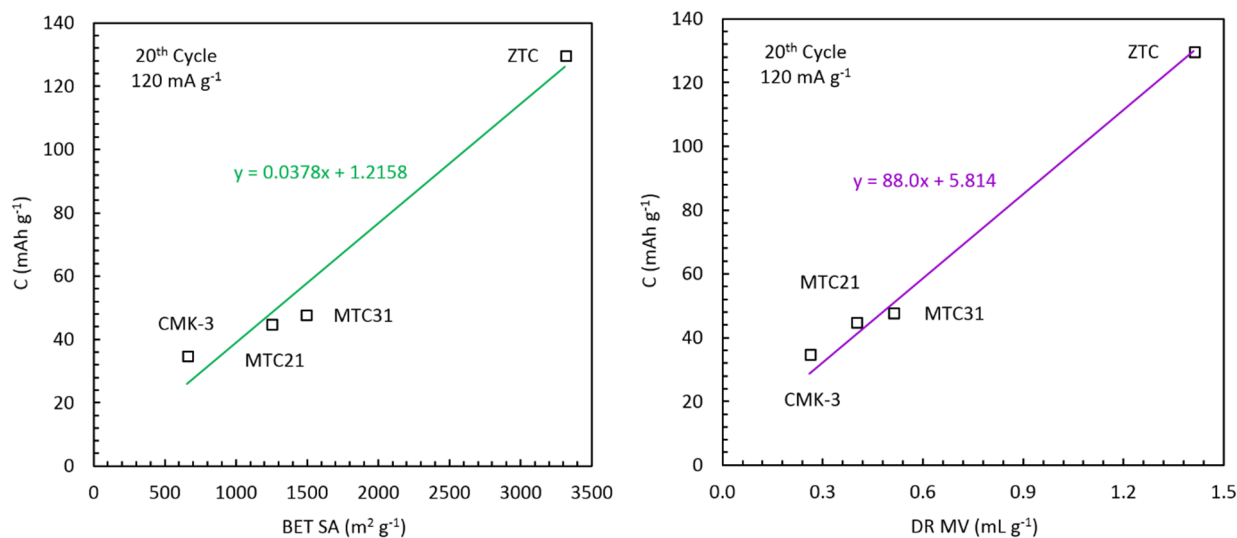


**Figure S6.** 20<sup>th</sup> cycle galvanostatic discharge capacity (between 2.65-4.7 V at 120 mA g<sup>-1</sup>) as a function of BET specific surface area (BET SA, left) and DR micropore volume (DR MV, right) for the porous carbon materials shown in **Figures S4-S5**, showing linear correlations corresponding to 37.8 mAh per 1000 m<sup>2</sup> (or 0.849 FSI<sup>-</sup> anions per nm<sup>2</sup>) of nitrogen-accessible surface and 88.0 mAh per mL (or 1.98 FSI<sup>-</sup> anions per nm<sup>3</sup>) of micropore volume. \*Note: the discharge capacity of ZTC at 120 mA g<sup>-1</sup> increases slightly to 141 mA g<sup>-1</sup> upon extended cycling.

## Electrolyte Concentration

The effects of altering the electrolyte concentration (KFSI in EC/DMC (1:1 by weight)) were assessed at up to 4.8 M (final electrolyte concentration); a comparison between 3.2 and 4.8 M solutions is shown in **Figure S7**.

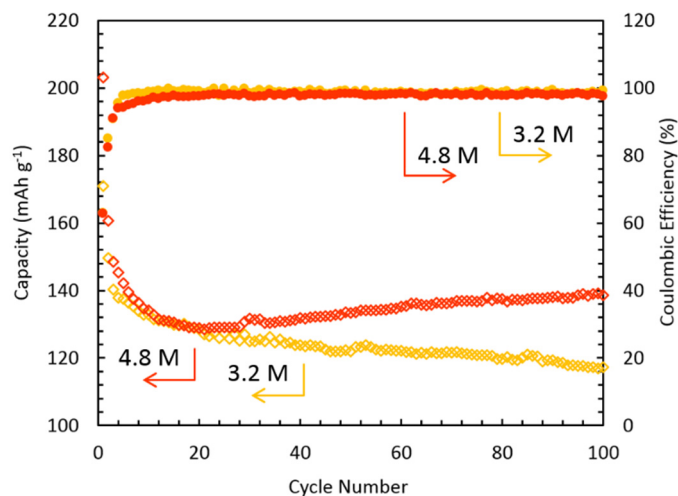


**Figure S7.** Discharge capacity retention (open diamonds) and coulombic efficiency (filled circles) over 100 cycles for ZTC KFSI DIBs cycled between 2.65-4.7 V at 120 mA g<sup>-1</sup>, in a low (3.2 M) and high (4.8 M) concentration electrolyte (KFSI in EC/DMC (1:1 by weight) solution).

## Electrochemical Stability Range of ZTC

It is important to note that in well-studied LIB systems, highly porous carbons such as ZTC have been demonstrated not to be suitable as anode materials owing to their reductive instability in the necessary potential range (typically 0.01-1.50 V) in the typical electrolytes employed, leading to a high irreversible capacity loss during the first cycle and to the consumption of excessive electrolyte to form SEI.<sup>S8,S9</sup> The continued cycling of such materials under the same conditions (after the formation of a protective SEI layer), however, has demonstrated their subsequent high reversible charge storage capacity (even up to >1000 mAh g<sup>-1</sup>)<sup>S10</sup>, but the large irreversible capacity in the first cycle must first be resolved in order to realize their promise as a high energy density electrode concept. To exploit the high adsorptive storage capacity of ZTC in an operational DIB, an appropriate voltage window must be established wherein the ZTC/electrolyte combination are co-stable. Such “stability ranges” for the reversible insertion/de-insertion of ions from several different electrolyte solutions have been previously reported for ZTC: -0.5 to 0.8 V vs. Ag/AgCl in 1 M H<sub>2</sub>SO<sub>4</sub> (2.75-4.05 V vs. Li/Li<sup>+</sup>)<sup>S11</sup>, -2.0 to 1.0 V vs. Ag/AgClO<sub>4</sub> in 1 M Et<sub>4</sub>NBF<sub>4</sub> in PC (1.85-4.25 V vs. Li/Li<sup>+</sup>)<sup>S12</sup>, and 1.2 to 4.7 V vs. Li/Li<sup>+</sup> in 1 M LiPF<sub>6</sub> in EC/DEC (1:1 by volume)<sup>S13</sup>, and 0.01 to 2.2 V vs. Al/Al<sup>3+</sup> in AlCl<sub>3</sub> in [EMIm]Cl (2.36-4.55 V vs. Li/Li<sup>+</sup>)<sup>S5</sup>. ZTC has no known range of stability in aqueous KOH nor in other alkaline aqueous electrolytes due to slow decomposition in the presence of OH<sup>-</sup>.<sup>S13</sup> Based on these results, ZTC is stable at relatively high voltages compared to lithium electroplating and stripping, and this also holds for sodium and more notably potassium (which differs from lithium by only ~0.1 V). Hence, it is reasonable to hypothesize that a high energy density lithium-, sodium-, or potassium-based DIB could be prepared using ZTC as the cathode when mated with an appropriate anion for reversible insertion/de-insertion within the high voltage window of stability.

## Cyclic Voltammetry

Cyclic voltammetry (CV) measurements were performed herein for two purposes: (a) to determine the optimal operating voltage range of electrochemical cells containing ZTC in the presence of KFSI (in EC/DMC) and (b) to classify the cathode material as either faradaic, pseudocapacitive, or capacitive, as recommended by Gogotsi and Penner<sup>S14</sup>. First, with respect to establishing the optimal operating window for ZTC in KFSI electrolyte, it is important to differentiate between the characteristics of the pristine material and that obtained after a pretreatment consisting of six very specific charge/discharge cycles (during which a certain quantity of FSI is irreversibly inserted into the pores of the ZTC), referred to thereafter as “cycled.” In all experiments described below, the electrolyte solution was 4.8 M KFSI in EC/DMC (1:1 by weight) as described in the Experimental Methods, and six cycles between 2.65-4.7 V vs. K/K<sup>+</sup> at 120 mA g<sup>-1</sup> were carried out to differentiate “cycled” ZTC from pristine ZTC.

The results of CV survey scans at 1 mV s<sup>-1</sup> on pristine and “cycled” ZTC are shown in **Figure S8**. For pristine ZTC, the CV scanning routine results in significant side reactions and therefore pseudocapacitive behavior even after extended cycling, especially below 1.2 V and above 4.5 V vs. K/K<sup>+</sup>. We attribute this behavior to the non-optimized formation of SEI during the initial electrochemical cycles. Hence, the ZTC cathode must first be electrochemically pretreated (*i.e.*, “cycled”), as described above, leading to optimal formation of SEI and thus optimal behavior of

the resulting KFSI DIB cells. This is inherently a trial-and-error process until the optimal pretreatment routine is established.

The results of CV survey scans at  $1 \text{ mV s}^{-1}$  on “cycled” ZTC, **Figure S8c-S8d**, demonstrate that the widest practical window of operation of ZTC is between 1.0-4.8 V vs.  $\text{K/K}^+$ . This result is directly comparable to and remarkably consistent with that for ZTC in 1 M  $\text{LiPF}_6$  in EC/DEC (1:1 by volume) as recently reported.<sup>S1</sup> However, this window is not the optimal range of operation for ZTC as the cathode in KFSI DIBs. Firstly, it was observed that the CE is significantly lower upon extended cycling above 4.7 V in full-cell DIBs, and hence an upper voltage limit of 4.7 V was established. The lower limit was established to prevent the insertion of  $\text{K}^+$  cations within the ZTC cathode and to ensure electroplating of potassium solely at the anode. A single discharge of “cycled” ZTC to 0 V vs.  $\text{K/K}^+$  was performed to determine this lower potential limit; the voltage as a function of time and the corresponding differential plot are shown in **Figure S9**. It can be seen that below 2.65 V vs.  $\text{K/K}^+$ , a rapid change in the current to potential differential occurs, indicating that potassium intercalation within ZTC begins. Hence, the optimal range of operation of a DIB cell employing ZTC as the cathode is 2.65-4.7 V vs.  $\text{K/K}^+$ .

Once this optimal range was established, slower CV scans were also performed at  $0.1 \text{ mV s}^{-1}$  on pristine and “cycled” ZTC, as shown in **Figure S10**. As expected, by comparing “cycled” and pristine ZTC it is clear that the pretreatment results in CV behavior that is essentially reversible after only a few subsequent cycles. A less expectable result, perhaps, is that the eventual reversible capacitance is measurably different for the pristine and “cycled” ZTC, which is a result of the difference between the six pretreatment cycles (which occur before the CV begins for “cycled” ZTC) and the first six cycles undertaken during the CV measurements (cycles 1-6 for pristine ZTC). In both cases, the reversible and nearly rectangular shape of the cyclic voltammograms indicate a purely capacitive charge-storage mechanism in ZTC.

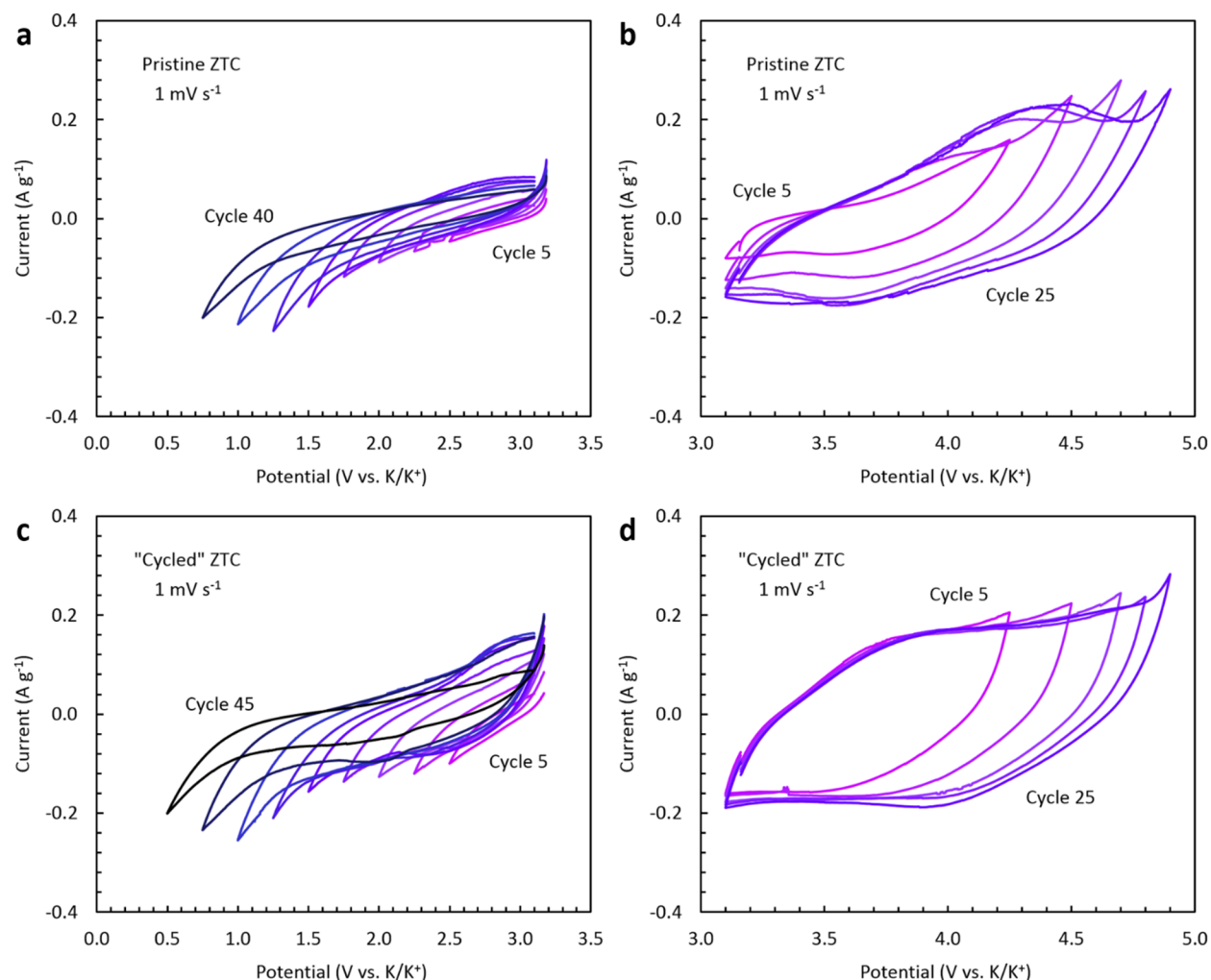


**Figure S8.** Cyclic voltammetry measurements of a KFSI DIB cell employing (a-b) pristine ZTC or (c-d) “cycled” ZTC as the active cathode material, within various voltage ranges to determine the optimal window of operation (reductive, (a) and (c), or oxidative, (b) and (d)), at a scan rate of  $1 \text{ mV s}^{-1}$ . Scans are shown in increasing cycle number from pink to black (note: for clarity, only every 5<sup>th</sup> scan is shown since 5 scans were performed within each tested potential range).

Samples are denoted as:

**Pristine ZTC:** cell prepared with bare, as-synthesized ZTC as the cathode material

**“Cycled” ZTC:** cell prepared with pre-cycled ZTC as the cathode material (pretreatment consisted of 6 charge/discharge cycles between 2.65-4.7 V vs.  $\text{K/K}^+$  at  $120 \text{ mA g}^{-1}$ )

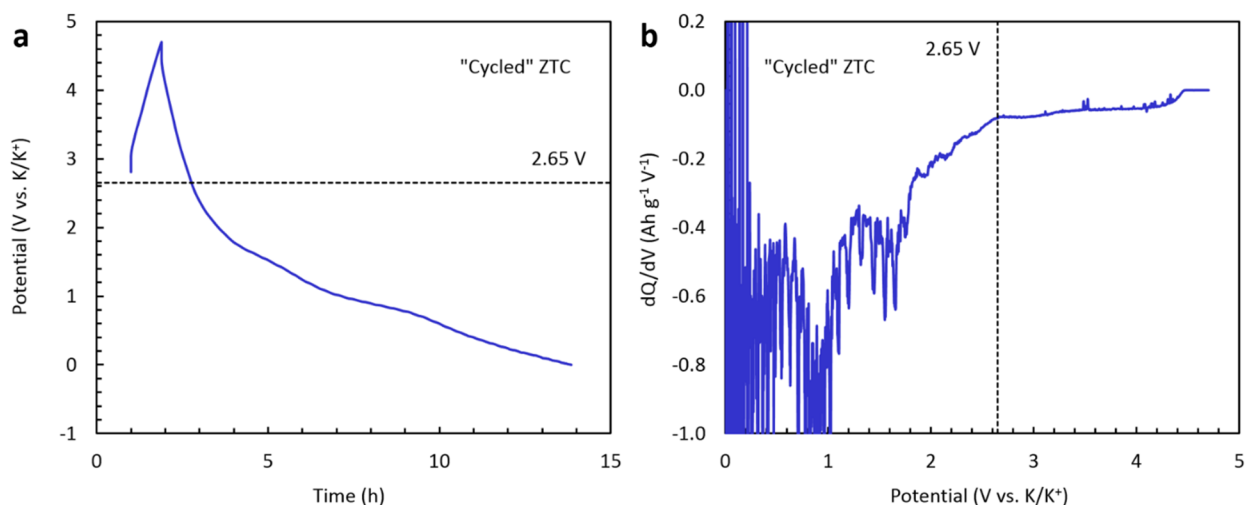


**Figure S9.** Single galvanostatic discharge experiment of a KFSI DIB cell employing “cycled” ZTC as the active cathode material starting from 4.7 V vs.  $\text{K}/\text{K}^+$ , showing (a) the cell potential as a function of time during the experiment and (b) the corresponding differential capacity plot.

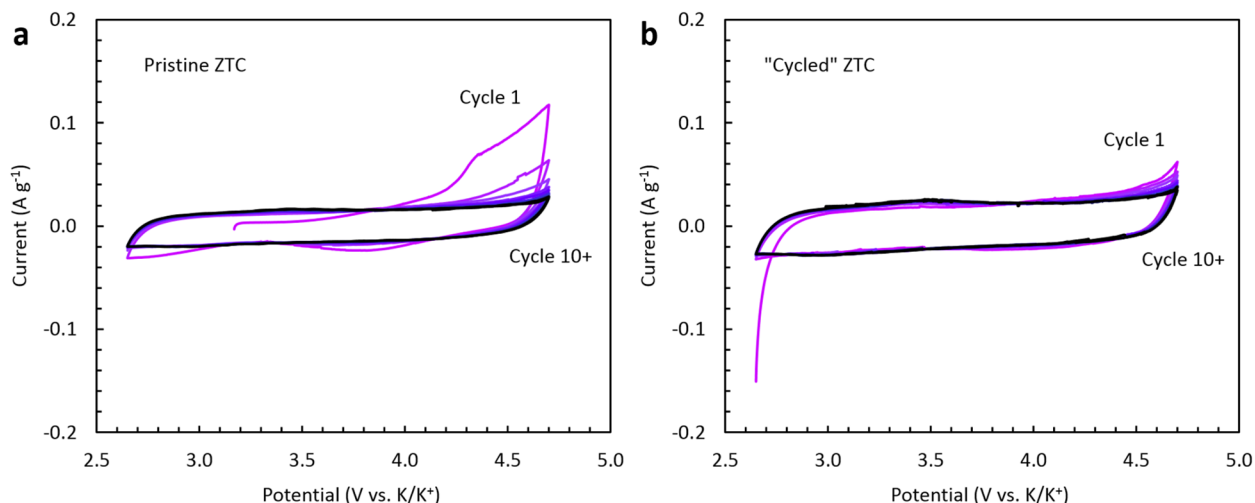


**Figure S10.** Cyclic voltammetry measurements of a KFSI DIB cell employing (a) pristine ZTC or (b) “cycled” ZTC as the active cathode material, between 2.65–4.7 V vs.  $\text{K}/\text{K}^+$  at a scan rate of  $0.1 \text{ mV s}^{-1}$ . All scans are shown with increasing cycle number from pink to black.

Samples are denoted as:

**Pristine ZTC:** cell prepared with bare, as-synthesized ZTC as the cathode material

**“Cycled” ZTC:** cell prepared with pre-cycled ZTC as the cathode material (pretreatment consisted of 6 charge/discharge cycles between 2.65–4.7 V vs.  $\text{K}/\text{K}^+$  at  $120 \text{ mA g}^{-1}$ )

Galvanostatic Cycling

Additional galvanostatic cycling was performed to characterize the voltage profiles of the six cycles undertaken during pretreatment between 2.65-4.7 V vs. K/K<sup>+</sup> at 120 mA g<sup>-1</sup> (*i.e.*, from pristine to “cycled” ZTC, **Figure S11**), and to explore ZTC as an anode material for K<sup>+</sup> insertion between 0-2.5 V vs. K/K<sup>+</sup> (**Figure S12**). In both experiments, the electrolyte solution was 4.8 M KFSI in EC/DMC (1:1 by weight) as described in Experimental Methods.

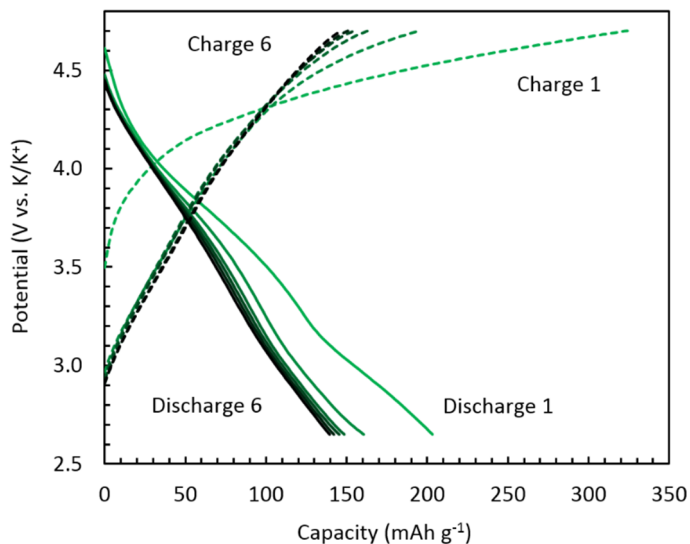


**Figure S11.** Galvanostatic charge/discharge voltage profiles of ZTC during pretreatment, at a current rate of 120 mA g<sup>-1</sup> (discharge shown as solid lines, charge shown as dashed lines).

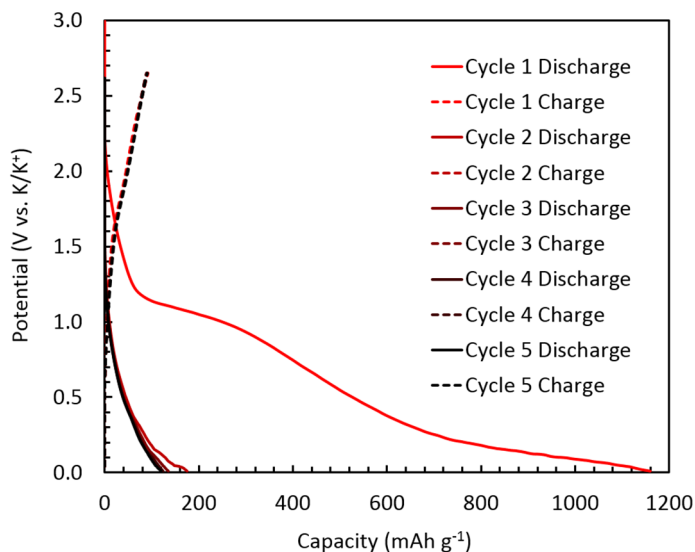


**Figure S12.** Galvanostatic charge/discharge voltage profiles of ZTC as an anode at a current rate of 120 mA g<sup>-1</sup> (discharge shown as solid lines, charge shown as dashed lines).  
NMR Characterization

Additional NMR characterization was performed as described in the Experimental Methods and the results are shown in **Figures S13-S14**. All experiments were performed on pristine ZTC, neat electrolyte (5 M KFSI in EC/DMC (1:1 by weight)), ex-situ samples of ZTC at various stages of electrochemical cycling in a KFSI DIB cell (where cycling was carried out six times, between 2.65-4.7 V vs. K/K<sup>+</sup>, at 120 mA g<sup>-1</sup>), or solution-impregnated samples of ZTC either before or after the described washing treatment to remove electrolyte from the surface of the ZTC particles. The washing procedure was carried out in a careful manner to prevent any change to the state of charge. The detailed measurement parameters are given in **Tables S1-S4**.

Samples are denoted as:

**Pristine ZTC**: uncycled, dry, as-prepared ZTC. Appearance: powder

**Impregnated ZTC (Unwashed)**: uncycled, as-prepared ZTC powder, immersed in 5 M KFSI in EC/DMC (1:1) and stirred for 2 h at room temperature, collected after centrifugation at 12000 rpm for 5 min. Appearance: slurry

**Impregnated ZTC (Washed)**: uncycled, as-prepared ZTC powder, immersed in 5 M KFSI in EC/DMC (1:1) and stirred for 2 h at room temperature, washed with three aliquots of EC/DMC (1:1, 3 mL), collected after centrifugation at 12000 rpm for 5 min, dried overnight under vacuum. Appearance: powder

**Fully Charged ZTC**: “cycled” ZTC, collected from 6 coin cells containing 5 mg ZTC each, removed from the DIB cell after a complete charge step to 4.7 V vs. K/K<sup>+</sup>, washed with three aliquots of EC/DMC (1:1, 3 mL), collected after centrifugation at 12000 rpm for 5 min, dried overnight under vacuum. Appearance: powder

**Fully Discharged ZTC**: “cycled” ZTC, collected from 6 coin cells containing 5 mg ZTC each, removed from the DIB cell after a complete discharge step to 2.65 V vs. K/K<sup>+</sup>, washed with three aliquots of EC/DMC (1:1, 3 mL), collected after centrifugation at 12000 rpm for 5 min, dried overnight under vacuum. Appearance: powder

**Electrolyte**: 5 M KFSI in EC/DMC (1:1 by weight). Appearance: solution

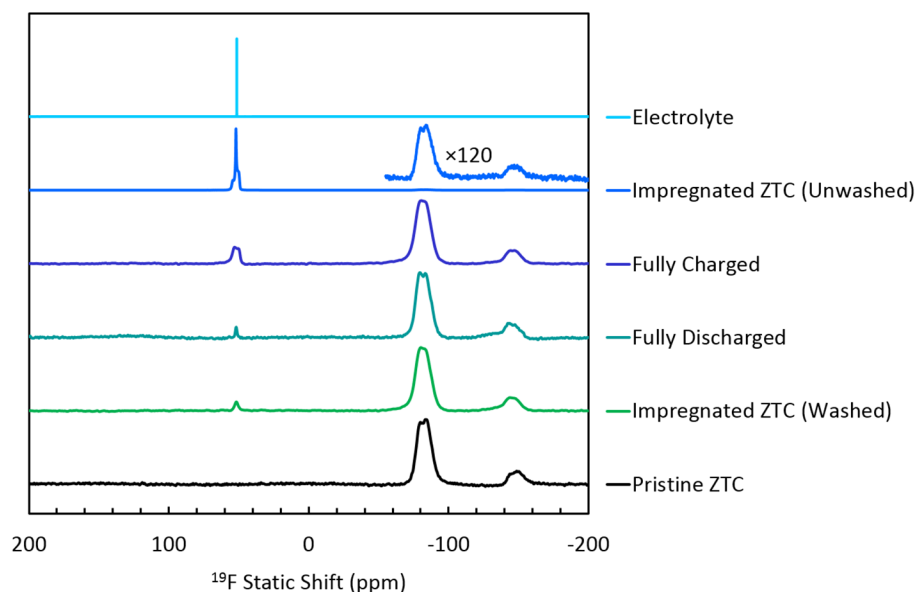


**Figure S13.**  $^{19}\text{F}$  static NMR spectra of pristine ZTC, neat electrolyte, and several ex-situ ZTC samples subjected to the treatments as described above. The signals at -84 and -148 ppm are due to instrument background. Despite thorough and careful washing, it was not possible to fully remove the liquid electrolyte from solution-impregnated ZTC, as revealed by the presence of a peak at 52 ppm in both samples. The minor variations in the linewidth of the signal at 52 ppm cannot be easily compared to MAS  $^{19}\text{F}$  spectra due to the presence of various dipolar interactions and altered electrolyte viscosities in the pores as a result of different sample preparation (*e.g.*, washing vs. vacuum drying). The spectrum from the charged ZTC sample does exhibit a stronger and much broader FSI $^-$  signal compared to that of the discharged ZTC.

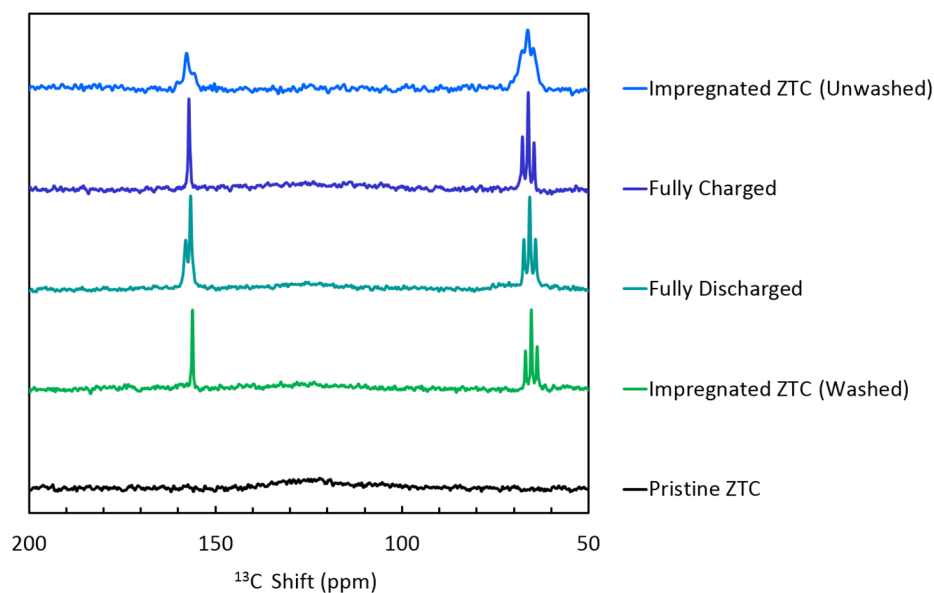


**Figure S14.**  $^{13}\text{C}$  MAS NMR spectra of pristine ZTC, neat electrolyte, and several ex-situ ZTC samples subjected to the treatments as described above (note: the unwashed sample could not be spun owing to excessive residual electrolyte and hence a static NMR spectrum is shown).

**Table S1.** Acquisition parameters for  $^{19}\text{F}$  static solid-state NMR (**Figure S13**)

Magnetic Field (T)	9.4
Temperature (K)	298
Rotor Diameter (mm)	2.5
Pulse Sequence	90°-one-pulse
Number of Scans	1024
Recycle Delay (s)	5
Spectral Width (kHz)	938
Spinning Frequency (Hz)	0
Acquisition Length (points)	10240
$^{19}\text{F}$ 90° Pulse Width [ $\pi/2$ ] ( $\mu\text{s}$ )	5.75

**Table S2.** Acquisition parameters for  $^{19}\text{F}$  solution-state NMR (“electrolyte,” **Figure S13**)

Magnetic Field (T)	11.7
Temperature (K)	298
Rotor Diameter (mm)	2.5
Pulse Sequence	90°-one-pulse
Decoupling Sequence	Inverse gated H-1 WALTZ16 decoupling
Number of Scans	256
Recycle Delay (s)	8
Spectral Width (kHz)	469
Spinning Frequency (Hz)	0
Acquisition Length (points)	11072

**Table S3.** Acquisition parameters for  $^{19}\text{F}$  solid-state MAS NMR measurements (**Figure 4**)

Magnetic Field (T)	9.4
Temperature (K)	298
Rotor Diameter (mm)	2.5
Pulse Sequence	90°-one-pulse
Number of Scans	1024
Recycle Delay (s)	5
Spectral Width (kHz)	938
Spinning Frequency (Hz)	0
Acquisition Length (points)	10240
$^{19}\text{F}$ 90° Pulse Width [ $\pi/2$ ] ( $\mu\text{s}$ )	5.75

**Table S4.** Acquisition parameters for  $^{13}\text{C}$  solid-state MAS NMR measurements (**Figure S14**)

Magnetic Field (T)	11.7
Temperature (K)	298
Rotor diameter (mm)	2.5
Pulse Sequence	30°-one-pulse
Number of Scans	256
Recycle Delay (s)	8
Spectral Width (kHz)	469
Spinning Frequency (Hz)	0
Acquisition Length (points)	11072

### Elemental Analysis

To support the solid-state NMR results which are not always quantitative due to small variations in packing of the rotor, micro-elemental analysis was performed on several ZTC samples (**Table S5**). Note: the Schöniger method bears a high error for halogen compositions of <1 wt%.<sup>S15</sup>

Samples are denoted as:

**Impregnated ZTC (Washed):** uncycled, as-prepared ZTC powder, immersed in 5 M KFSI in EC/DMC (1:1) and stirred for 2 h at room temperature, washed with three aliquots of EC/DMC (1:1, 3 mL), collected after centrifugation at 12000 rpm for 5 min, dried overnight under vacuum. Appearance: powder

**Fully Charged ZTC:** “cycled” ZTC, collected from 6 coin cells containing 5 mg ZTC each, removed from the DIB cell after a complete charge step to 4.7 V vs. K/K<sup>+</sup>, washed with three aliquots of EC/DMC (1:1, 3 mL), collected after centrifugation at 12000 rpm for 5 min, dried overnight under vacuum. Appearance: powder

**Fully Discharged ZTC:** “cycled” ZTC, collected from 6 coin cells containing 5 mg ZTC each, removed from the DIB cell after a complete discharge step to 2.65 V vs. K/K<sup>+</sup>, washed with three aliquots of EC/DMC (1:1, 3 mL), collected after centrifugation at 12000 rpm for 5 min, dried overnight under vacuum. Appearance: powder

**Table S5.** Elemental analysis of solution-impregnated and electrochemically cycled ZTC, performed in duplicate (both individual results shown).

Element	Impregnated ZTC (Washed)	Fully Charged ZTC	Fully Discharged ZTC
	Content (wt%)	Content (wt%)	Content (wt%)
Carbon	50.03/49.91	42.26/42.39	43.38/43.38
Hydrogen	4.13/4.14	4.34/4.38	4.28/4.19
Nitrogen	0.17/0.19	0.25/0.27	0.18/0.18
Sulfur	0.09/0.01	1.02/0.90	0.46/0.47
Fluorine	0.13/0.09	0.42/0.41	0.46/0.47

In all samples, a high content of elements other than C, H, N, S, and F was observed (see **Figure S15**), which is most likely due to the presence of oxygen, aluminum, and silicon (originating from the zeolite template and/or the glass fiber separator used for electrochemical cell fabrication). The sulfur content of fully charged ZTC is double that of fully discharged ZTC, which gives further quantitative evidence for the electrochemical insertion of FSI<sup>-</sup> within ZTC to that given by NMR.

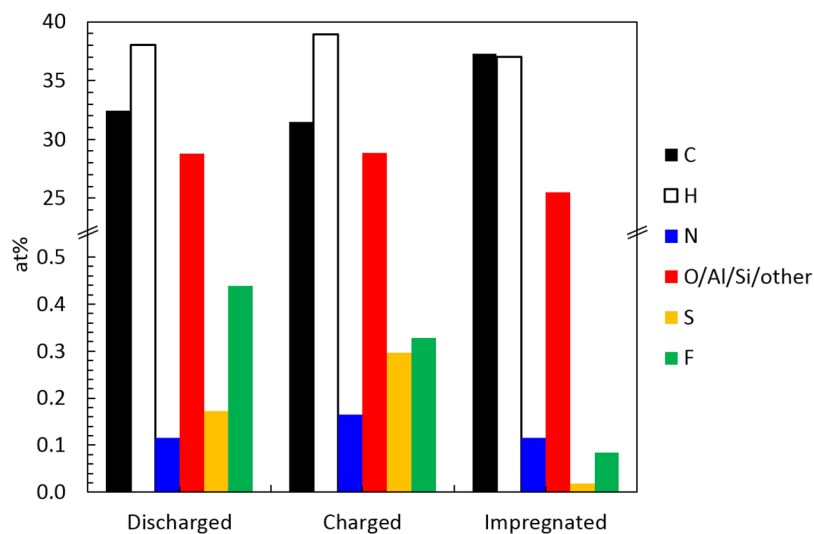


**Figure S15.** Elemental composition analysis of ex-situ ZTC samples subjected to the treatments described above. The “other” content (red) found by subtracting the CHNSF components from 100% likely contains oxygen in addition to aluminum and silicon (*e.g.*, from the zeolite, quartz synthesis tube, or glass fiber separator). Note: there is a relatively large error associated with the fluorine content.

## Energy and Power Density Calculations

The specific energy of a cathode depends crucially on both the reversible charge capacity and voltage difference from the anode. Along the discharge voltage profile,  $V_{dis}(I)$ :

$$E = \int V_{dis}(Q) dQ \quad \text{Equation S1}$$

Then the average discharge voltage is found by dividing the total specific energy by the total discharge capacity of the charge storage material:

$$V_{avg} = \frac{E}{Q_{max}} \quad \text{Equation S2}$$

Lastly, specific power is determined by multiplying the average discharge voltage by the current rate (which is constant over the galvanostatic voltage profile):

$$P = V_{avg} \cdot I \quad \text{Equation S3}$$

The energy and power densities of the four porous carbons investigated in this work are shown in **Figure S16**, as a function of both specific surface area and current rate.

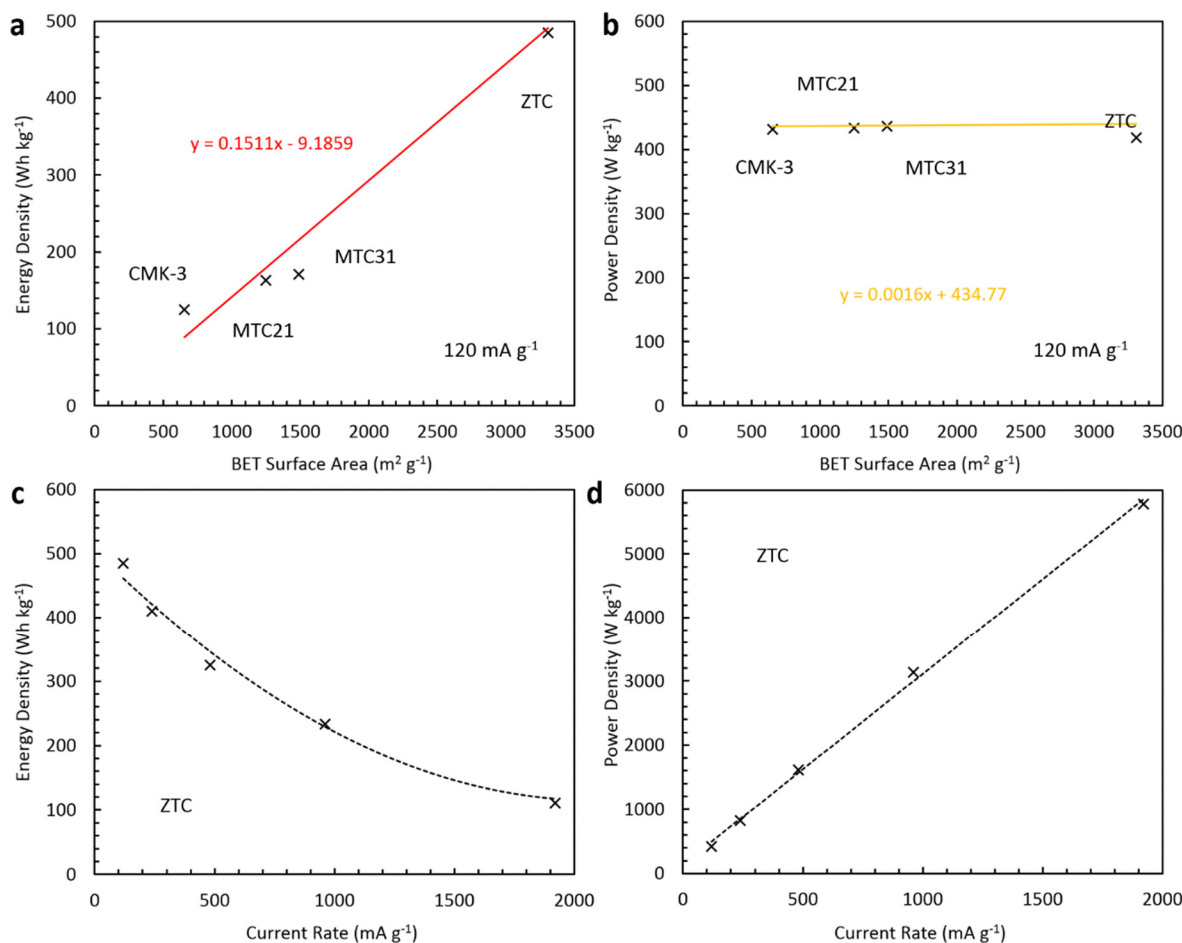


**Figure S16.** Cathode-specific energy and power density as a function of BET surface area (a-b, respectively) and current rate (c-d, respectively) of the carbon materials shown in **Figures S4-S5**.

## Cathode to Full-Cell Conversions

To determine the energy and power density of a full-cell KFSI DIB (based on a particular specific energy and power density of the porous carbon cathode), one must take into consideration the necessary mass (or volume) of the electrolyte solution, containing active  $K^+$  and  $FSI^-$  ions as well as solvent. There is additional mass and volume associated with the stainless-steel case, current collectors, and separator, but these will be considered in less detail herein.

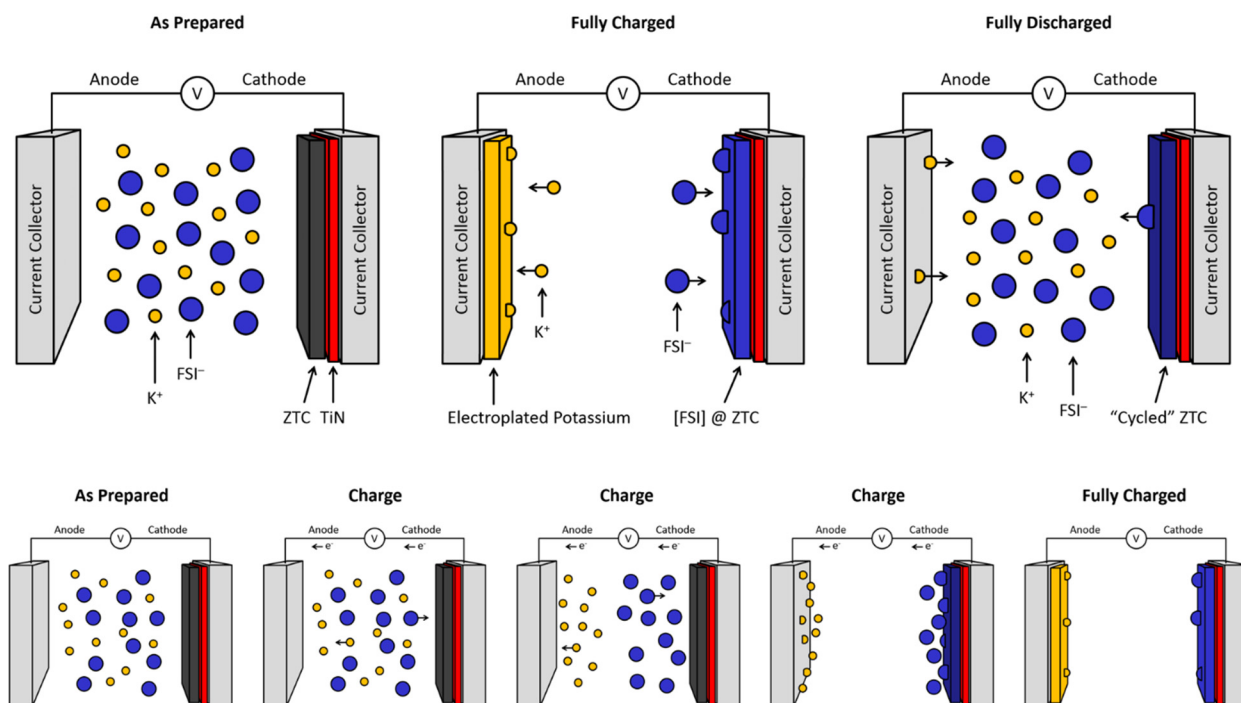


**Figure S17.** Schematic depiction of the working principle of a KFSI DIB employing ZTC as the active cathode material and the electroplating/stripping reaction at the anode, as shown in fully charged and discharged states (top) and during the process of charging (bottom).

During charging (see **Figure S17**), the KFSI DIB undergoes electroplating of potassium from the solution containing  $K^+$  cations at the anode. A thin film of potassium covers the current collector before the first charge (of negligible mass and volume); otherwise, there is no inherent mass associated with the potassium “anode” itself. Hence, we refer to the neat electrolyte solution (containing  $K^+$  and  $FSI^-$ , along with solvent molecules) as the anode in the following discussion.

The relevant electrochemical reactions at the anode and the cathode are:



The absolute state of charge of a full-cell KFSI DIB is defined by the state of charge of either the anode or the cathode, since:

$$Q_{fc} = Q_a = Q_c \quad \text{Equation S6}$$

where  $Q_{fc}$ ,  $Q_a$ , and  $Q_c$  are the absolute charge of the full-cell, anode, and cathode, respectively. As described above, the “anode” refers to the electrolyte solution herein. In terms of the specific gravimetric charge capacity,  $C$ , and mass,  $m$ , of each component or the full-cell, the absolute charges can be rewritten as:

$$Q_{fc} = m_{fc} C_{fc} = (m_a + m_c + m_{extra}) C_{fc} \quad \text{Equation S7}$$

$$Q_a = m_a C_a \quad \text{Equation S8}$$

$$Q_c = m_c C_c \quad \text{Equation S9}$$

In the following work, each of the specific gravimetric charge capacities in these equations are given in units of mAh g<sup>-1</sup> and the masses are given in units of g. The “extra” mass,  $m_{extra}$ , is associated with the case, current collectors, and separator. These equations can be combined with Equation S6 to obtain the specific gravimetric charge capacity of the full-cell:

$$C_{fc} = \frac{Q_{fc}}{(m_a + m_c + m_{extra})} = \frac{Q_c}{(m_a + m_c + m_{extra})} = \frac{m_c C_c}{(m_a + m_c + m_{extra})} \quad \text{Equation S10}$$

For a full-cell KFSI DIB containing a fixed amount of cathode material (*e.g.*, ZTC) and operating under known conditions to achieve a specific cathodic charge capacity,  $C_c$ , all of the quantities in Equation S10 are known or measured except the minimum necessary mass of the anode. This is found by relating the concentration of the electrolyte to the charge capacity via:

$$C_a = \frac{Q_a}{m_a} = \frac{xF}{MW_a} \quad \text{Equation S11}$$

where  $F = 26.8 \times 10^3$  mAh mol<sup>-1</sup> (the Faraday constant),  $x$  is the ionic charge of the relevant electroactive species, and  $MW_a$  is the molar mass of the entire “anode” solution in g mol<sup>-1</sup>. In this case, the electroactive material is the KFSI salt dissolved in EC/DMC as the solvent. The molar mass depends on the state of charge of the cell, since in the fully charged state the electrolyte solution has a different composition than in the charged state. The average molar mass is found as follows:

$$MW_a = \frac{\rho_a \times 10^3}{M_{discharged} - M_{charged}} \quad \text{Equation S12}$$

where  $M$  is the molarity in mol L<sup>-1</sup> of the electrolyte in the discharged ( $M_{discharged}$ ) and charged ( $M_{charged}$ ) states, and  $\rho_a$  is the initial (as-prepared) density of the electrolyte in units of g mL<sup>-1</sup>.

Then, combining Equations S6, S8, S11, and S12:

$$m_a = \frac{Q_a}{C_a} = \frac{Q_c}{C_a} = \frac{C_c m_c}{C_a} = \frac{C_c m_c}{xF} \frac{\rho_a \times 10^3}{M_{discharged} - M_{charged}} \quad \text{Equation S13}$$

The measured density of the optimal electrolyte in this work (4.84 M KFSI in EC/DMC in a 1:1 ratio by weight) is  $\rho_a = 1.64 \text{ g mL}^{-1}$ . Correspondingly, the difference in molarity between the charged and discharged states is 4.84 M. Each of the electroactive ions in the solution has a single unit of charge ( $x = 1$ ). Lastly, the mass of “extra” components is taken to be a constant value of 5 mg (including a 2 mg case, two 1 mg current collectors, and a 1 mg separator) for a representative coin-type cell containing 25 mg of ZTC (and therefore ~30-40 mg of electrolyte, as shown in **Table S6a** and **Figure S18**). While these values are not necessarily representative of actual device characteristics, they are used herein for comparison to previous work.<sup>S5</sup>

The full-cell specific gravimetric energy density is then:

$$E_{fc} = V_{avg} C_{fc} \quad \text{Equation S14}$$

These quantities, in addition to full-cell specific gravimetric power densities (calculated as in Equation S3), are shown in **Table S6b**.

In addition to the above treatment, and for explicit comparison to other work where the mass of the “extra” components is neglected, we also calculate an “ideal” full-cell specific gravimetric energy and power density where  $m_{extra}$  is set equal to zero, using:

$$C_{fc,ideal} = \frac{m_c C_c}{(m_a + m_c)} = \frac{C_a C_c}{C_a + C_c} = \frac{xF(M_{discharged} - M_{charged})C_c}{xF(M_{discharged} - M_{charged}) + C_c \rho_a \times 10^3} \quad \text{Equation S15}$$

The corresponding ideal specific gravimetric energy and power densities of ZTC are shown in **Table S6c**.

The average voltage and specific gravimetric charge capacity at the cathode depend on the current rate utilized, and the energy density therefore varies as shown in **Tables S6b-S6c**. The corresponding specific volumetric energy and power densities are found by using the measured tap density of each material (and maximum density of hot-pressed ZTC as reported by Hou et al.<sup>S16</sup>), as shown in **Tables S7-S9**. All specific volumetric full-cell quantities are calculated based on the tap density volume of ZTC and the average electrolyte volume only, and hence a negligible additional volume for the “extra” components of the DIB cell.

\*Note:  $C$  is used in the above equations to denote “capacity”, not the unit of “coulombs”.

**Table S6a.** Specific gravimetric capacity of ZTC as the cathode in a KFSI DIB full-cell and corresponding necessary mass of electrolyte (4.8 M KFSI in EC/DMC in a 1:1 ratio by weight) at varying current rates.

Current Rate (mA g <sup>-1</sup> )	Cathodic Capacity (mAh g <sup>-1</sup> )	Required Electrolyte Amount	
		m <sub>a</sub> /m <sub>c</sub> (g <sub>a</sub> g <sub>c</sub> <sup>-1</sup> )	m <sub>a</sub> (mg <sub>a</sub> per 25 mg <sub>c</sub> )
120	139.2	1.760	44.0
240	119.9	1.516	37.9
480	96.8	1.224	30.6
960	71.5	0.904	22.6
1920	36.9	0.467	11.68

**Table S6b.** Specific gravimetric capacity, average voltage, energy density, and power density of a ZTC cathode and the corresponding KFSI DIB full-cell (containing 25 mg of ZTC and 5 mg of “extra” components) at varying current rates. The used capacities stem from the 10<sup>th</sup>, 15<sup>th</sup>, 20<sup>th</sup>, 25<sup>th</sup>, and 30<sup>th</sup> cycle in **Figure 3d**.

Current Rate (mA g <sup>-1</sup> )	Cathodic Capacity (mAh g <sup>-1</sup> )	Average Voltage (V)	Cathode Specific		Full-Cell (m <sub>extra</sub> = 5 mg)	
			Energy Density (Wh kg <sub>c</sub> <sup>-1</sup> )	Power Density (W kg <sub>c</sub> <sup>-1</sup> )	Energy Density (Wh kg <sub>c</sub> <sup>-1</sup> )	Power Density (W kg <sub>c</sub> <sup>-1</sup> )
120	139.2	3.483	484.8	418.0	163.8	141.2
240	119.9	3.417	409.7	820.1	150.9	302.0
480	96.8	3.353	324.6	1609	133.9	664.0
960	71.5	3.261	233.2	3131	110.8	1488
1920	36.9	3.013	111.2	5785	66.7	3471

**Table S6c.** Specific gravimetric capacity, average voltage, energy density, and power density of a ZTC cathode and the corresponding “idealized” KFSI DIB full-cell (with negligible mass of “extra” components) at varying current rates.

<b>Current Rate</b> (mA g <sup>-1</sup> )	<b>Cathodic Capacity</b> (mAh g <sup>-1</sup> )	<b>Average Voltage</b> (V)	<b>Cathode Specific</b>		<b>Full-Cell (m<sub>extra</sub> = 0)</b>	
			<b>Energy Density</b> (Wh kg <sup>-1</sup> )	<b>Power Density</b> (W kg <sup>-1</sup> )	<b>Energy Density</b> (Wh kg <sup>-1</sup> )	<b>Power Density</b> (W kg <sup>-1</sup> )
120	139.2	3.483	484.8	418.0	175.7	151.4
240	119.9	3.417	409.7	820.1	162.8	326.0
480	96.8	3.353	324.6	1609	146.0	723.7
960	71.5	3.261	233.2	3131	122.5	1644
1920	36.9	3.013	111.2	5785	75.8	3945

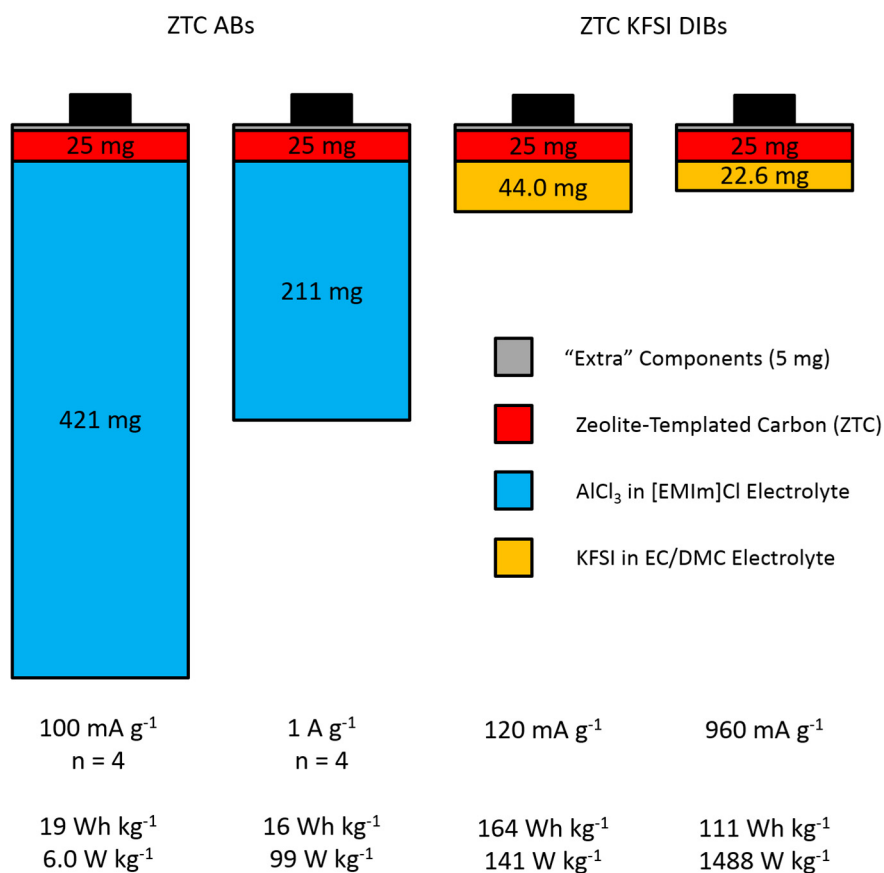


**Figure S18.** Mass-scaled diagrams of aluminum battery (AB) and KFSI dual-ion battery (DIB) full-cells based on ZTC as the cathode (25 mg) and either  $\text{AlCl}_3$  in  $[\text{EMIm}]\text{Cl}$  ( $r = 1.3$ )<sup>S5</sup> or KFSI in EC/DMC (4.8 M) as the electrolyte (of variable mass). An estimated mass of “extra” components (the cell case, current collectors, and separator) is also added. The amount of electrolyte required depends on the reversible capacity of the ZTC cathode (which varies as a function of current rate, see **Figure 3c**) and, in the case of ZTC ABs<sup>S5</sup>, the mechanism of charge storage (the conventional mechanism corresponding to  $n = 4$  is used here for simplicity). The energy and power density depend on the average operating voltage of the cell, which is 1.05 V (vs.  $\text{Al}/\text{Al}^{3+}$ ) for ZTC ABs and 3.0-3.5 V (vs.  $\text{K}/\text{K}^+$ ) for ZTC KFSI DIBs. Note: actual full-cells prepared in this work contained  $\leq 5$  mg ZTC.

**Table S7.** Bulk material densities used in gravimetric to volumetric capacity calculations.

Material	Density (g mL <sup>-1</sup> )	Reference
ZTC	0.2	(measured)
Densified ZTC	0.9	Hou et al. <sup>S16</sup>

Cathode-specific volumetric capacity, energy density, and power density are simply determined by an equation of type:

$$C_{c,vol} = C_c \times \rho_c \quad \text{Equation S16}$$

where the density of the cathode,  $\rho_c$ , depends significantly on whether the material is densified prior to preparation of the cells (see **Table S7**). The corresponding full-cell energy and power densities are determined based on the volume of the electrolyte (anode) and ZTC (cathode), with no contribution from the volume of “extra” components, via an equation of type:

$$E_{fc,vol} = \frac{E_{fc}(m_a + m_c)}{(V_a + V_c)} = \frac{E_{fc}(m_a + m_c)}{\left(\frac{C_c m_c}{x F M_{discharged} - M_{charged}} + \frac{m_c}{\rho_c \times 1000}\right)} \quad \text{Equation S16}$$

**Table S8.** Specific volumetric capacity, average voltage, energy density, and power density of a ZTC cathode (0.2 g mL<sup>-1</sup>) and the corresponding KFSI DIB full-cell at varying current rates.

Current Rate (mA g <sup>-1</sup> )	Cathodic Capacity (Ah L <sub>c</sub> <sup>-1</sup> )	Average Voltage (V)	Cathode Specific		Full-Cell (V <sub>extra</sub> = 0)	
			Energy Density (Wh L <sub>c</sub> <sup>-1</sup> )	Power Density (W L <sub>c</sub> <sup>-1</sup> )	Energy Density (Wh L <sub>fc</sub> <sup>-1</sup> )	Power Density (W L <sub>fc</sub> <sup>-1</sup> )
120	27.8	3.483	97.0	83.6	79.8	68.8
240	24.0	3.417	81.9	164.0	69.2	138.4
480	19.4	3.353	64.9	321.9	56.5	280.1
960	14.3	3.261	46.6	626.1	42.0	563.9
1920	7.38	3.013	22.2	1157	21.0	1095

**Table S9.** Specific volumetric capacity, average voltage, energy density, and power density of an optimally densified ZTC cathode (0.9 g mL<sup>-1</sup>) and the corresponding KFSI DIB full-cell at varying current rates.

Current Rate (mA g <sup>-1</sup> )	Cathodic Capacity (Ah L <sub>c</sub> <sup>-1</sup> )	Average Voltage (V)	Cathode Specific		Full-Cell (V <sub>extra</sub> = 0)	
			Energy Density (Wh L <sub>c</sub> <sup>-1</sup> )	Power Density (W L <sub>c</sub> <sup>-1</sup> )	Energy Density (Wh L <sub>fc</sub> <sup>-1</sup> )	Power Density (W L <sub>fc</sub> <sup>-1</sup> )
120	125.3	3.483	436.4	376.2	222.0	191.4
240	107.9	3.437	368.7	738.1	201.3	402.9
480	87.1	3.399	292.1	1448	174.7	866.5
960	64.4	3.261	209.8	2818	140.3	1883
1920	33.2	3.013	100.0	5206	79.7	4145

## Supporting References

- S1. H. Nishihara, T. Kyotani, *Chem. Commun.* **2018**, 54, 5648.
- S2. Z. Ma, T. Kyotani, A. Tomita, *Carbon* **2002**, 40, 2367.
- S3. K. Matsuoka, Y. Yamagishi, T. Yamazaki, N. Setoyama, A. Tomita, T. Kyotani, *Carbon* **2005**, 43, 855.
- S4. H. Nishihara, H. Fujimoto, H. Itoi, K. Nomura, H. Tanaka, M. T. Miyahara, P. A. Bonnaud, R. Miura, A. Suzuki, N. Miyamoto, *Carbon* **2018**, 129, 854.
- S5. N. P. Stadie, S. Wang, K. V. Kravchyk, M. V. Kovalenko, *ACS Nano* **2017**, 11, 1911.
- S6. F. Rouquerol, J. Rouquerol, K. S. W. Sing, *Adsorption by Powders and Porous Solids: Principles, Methodology, and Applications*, Academic Press, San Diego, **1999**.
- S7. J. Rouquerol, P. Llewellyn, F. Rouquerol, *Stud. Surf. Sci. Catal.* **2007**, 160, 49.
- S8. C. J. Meyers, S. D. Shah, S. C. Patel, R. M. Sneeringer, C. A. Bessel, N. R. Dollahon, R. A. Leising, E. S. Takeuchi, *J. Phys. Chem. B* **2001**, 105, 2143.
- S9. H. Nishihara, T. Kyotani, *Adv. Mater.* **2012**, 24, 4473.
- S10. Y. Lv, Z. Wu, X. Qian, Y. Fang, D. Feng, Y. Xia, B. Tu, D. Zhao, *ChemSusChem* **2013**, 6, 1938.
- S11. H. Itoi, H. Nishihara, T. Ishii, K. Nueangnoraj, R. Berenguer-Betrián, T. Kyotani, *Bull. Chem. Soc. Jpn.* **2014**, 87, 250.
- S12. K. Nueangnoraj, H. Nishihara, T. Ishii, N. Yamamoto, H. Itoi, R. Berenguer, R. Ruiz-Rosas, D. Cazorla-Amorós, E. Morallón, M. Ito, T. Kyotani, *Energy Storage Mater.* **2015**, 1, 35.
- S13. H. Nishihara, T. Kyotani, *Chem. Commun.* **2018**, 54, 5648.
- S14. Y. Gogotsi, R. M. Penner, *ACS Nano* **2018**, 12, 2081.
- S15. W. Schöniger, *Microchim. Acta* **1956**, 44, 869.
- S16. P.-X. Hou, H. Orikasa, H. Itoi, H. Nishihara, T. Kyotani, *Carbon* **2007**, 45, 2011.